Supplementary Information for

Size-Tunable Synthesis of Monolayer MoS_2 Nanoparticles and Their Applications in Non-Volatile Memory Devices

Jaeho Jeon[a], Jinhee Lee[b], Gwangwe Yoo[c], Jin-Hong Park[c], Geun Young Yeom[d], Yun Hee Jang[b,e], and Sungjoo Lee[a,c*]*

[a]*SKKU Advanced Institute of Nanotechnology (SAINT), Sungkyunkwan University (SSKU), Suwon 440-746, Korea. E-mail: leesj@skku.edu*

[b]*School of Materials Science and Engineering, Gwangju Institute of Science and Technology, Gwangju 550-712, Korea. E-mail: yhjang@gist.ac.kr*

[c]*School of Electronics and Electric Engineering, Sungkyunkwan University (SKKU), Suwon 440-746, Korea.*

[d]*School of Advanced Materials Science and Engineering, Sungkyunkwan University (SKKU), Suwon, 440-746, Korea.*

[e]*Department of Energy Systems Engineering, DGIST, Daegu 42988, Korea*

Surface Morphologies of the MoS_2 Nanoparticles: The shapes and thicknesses of our CVD-grown size-tunable MoS_2 nanoparticles were characterized using AFM measurements. Supplementary Figure S1(a) shows the triangular MoS_2 nanoparticles grown under pure Ar gas. The largest nanoparticle size obtained under these conditions was 100 nm due to the typical sulfurization growth of molybdenum oxide and the high chemical potential of sulfur (μ_s). As hydrogen gas was injected during the growth of MoS_2 nanoparticles, the nanoparticle size decreased to 40 nm, 18 nm, or 6 nm, as shown in Supplementary Figure S1(b), S1(c), and S1(d) under the gas flow conditions: Ar 60 sccm–H_2 30 sccm , Ar 60 sccm–H_2 30 sccm, and H_2 90 sccm, respectively. Most CVD-grown MoS_2 nanoparticles were 0.7–1 nm thick, comparable to the monolayer MoS_2 thickness. These measured values also agreed with the Raman spectra. Figure S2 shows the Raman spectra collected from the MoS_2 nanoparticles grown under different hydrogen gas flow rates. The normalized Raman spectrum from each nanoparticle displays two peaks at 385 cm^{-1} (E^1_{2g}: in-plane vibration of the Mo and S atoms) and 405 cm^{-1} (A^1_g: out-of-plane vibration of the Mo and S atoms). These results agree well with reported values for exfoliated MoS_2[1], suggesting that the MoS_2 nanoparticles have similar phonon–vibration characteristics even in crystals smaller than 10 nm in size. The difference between the wavenumbers of these two modes represents the number of MoS_2 layers present[1]. The difference between the E^1_{2g} and A^1_g peak positions in the Raman spectra, shown in the inset of Figure S2, is 19.6 cm^{-1}, in

agreement with previously reports of monolayer MoS_2[1]. The normalized Raman intensities of the two peaks decrease as the particle size decreases, due to a decrease in the phonon–vibration coupling strength within the small crystals[2].

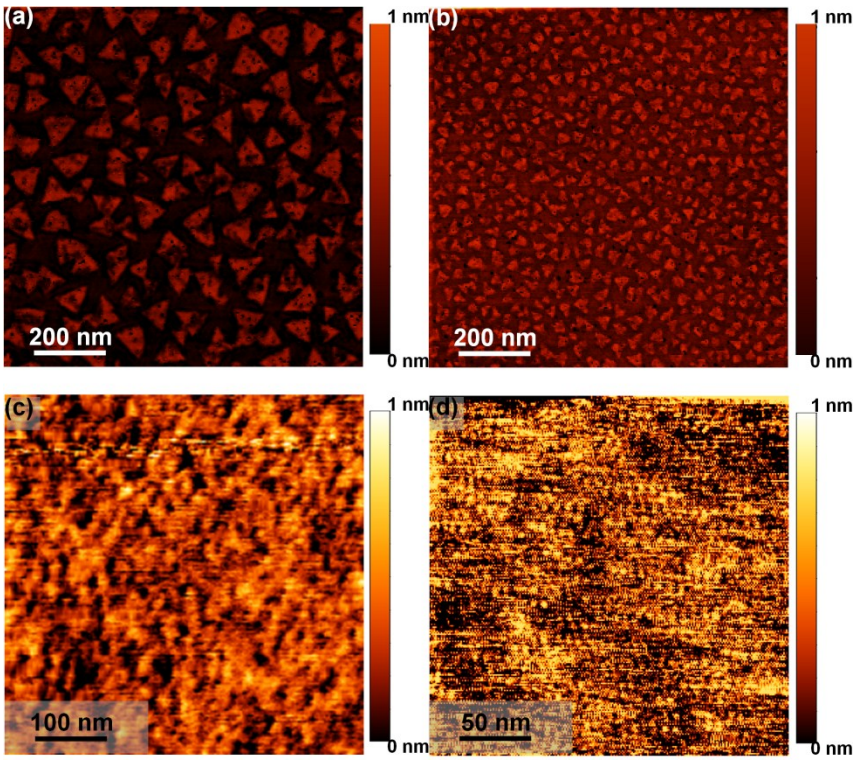

Figure S1. AFM measurements of the CVD-grown size-controlled MoS_2 nanoparticles grown under different conditions: (a) 50–70 nm MoS_2 nanoparticles grown in the absence of H_2, (b) 30–60 nm MoS_2 nanoparticles grown under 30 sccm H_2, (c) 10–30 nm MoS_2 nanoparticles grown under 60 sccm H_2, (d) 2–10 nm MoS_2 nanoparticles grown under 90 sccm H_2.

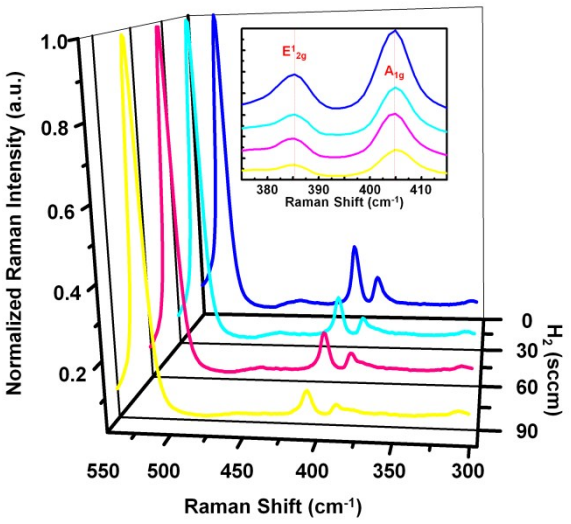

Figure S2. Raman spectra of the CVD-synthesized MoS_2 nanoparticles of different sizes, prepared under different H_2 gas flow rate conditions: full Raman spectra obtained from each sample, and enlarged Raman spectra (inset).

Chemical Configuration of the Molybdenum Oxysulfide: The chemical configurations of the MoS_2 nanoparticles were studied using XPS analysis. An abundance of hydrogen drove the oxidation of Mo atoms at the edge sites, as demonstrated by the Mo 3d and S 2p XPS spectra. Supplementary Figure S3 shows the deconvoluted O 1s XPS spectra obtained under the various H_2 flow rate conditions. The red curve indicates the full O 1s spectral shape, and the blue, green, and purple areas indicate Si-O bonding, Mo^{+6}-O bonding, and Mo^{+4}-O bonding. The binding energy of molybdenum oxide varied with the number of bonded oxygen atoms, yielded O 1s binding energies of 530.9 eV and 529.9 eV for MoO_3 and MoO_2, respectively[3]. The O 1s biding energies in molybdenum oxysulfide (MoS_xO_{3-x} or $MoS_{2x}O_x$) were expected to decrease due to instabilities in the metal-oxysulfide states. The 0 sccm and 30 sccm H_2 flow rate conditions (Supplementary Figures S3 (a) and (b)) provided one small metal oxygen peak at 531 eV. This O 1s peak was reflective of MoS_xO_{3-x} on the edges of the MoS_2 nanoparticles. The peak corresponding to Mo^{+6}-O bonding provided a very low contribution for two reasons: 1. the fraction of the relatively large MoS_2 nanoparticles corresponding to edges was low, and 2. sulfo-reduction under low H_2 concentrations was low. The peak intensity corresponding to Mo^{+6}-O bonding increased due to large proportion of edges and the extensive oxidation at the edges of the MoS_2 nanoparticles under the H_2 flow rate condition (Supplementary Figures S3(c) and (d)). Supplementary Figure S3 (d) revealed an additional metal-oxide binding peak at 529.3 eV corresponding to the Mo^{+4}-O bonding state in $MoS_{2-x}O_x$. The presence of Mo^{+4}-O bonds indicated that the basal plane of the MoS_2 nanoparticles was oxidized due to extensive sulfur reduction under abundant H_2 conditions.

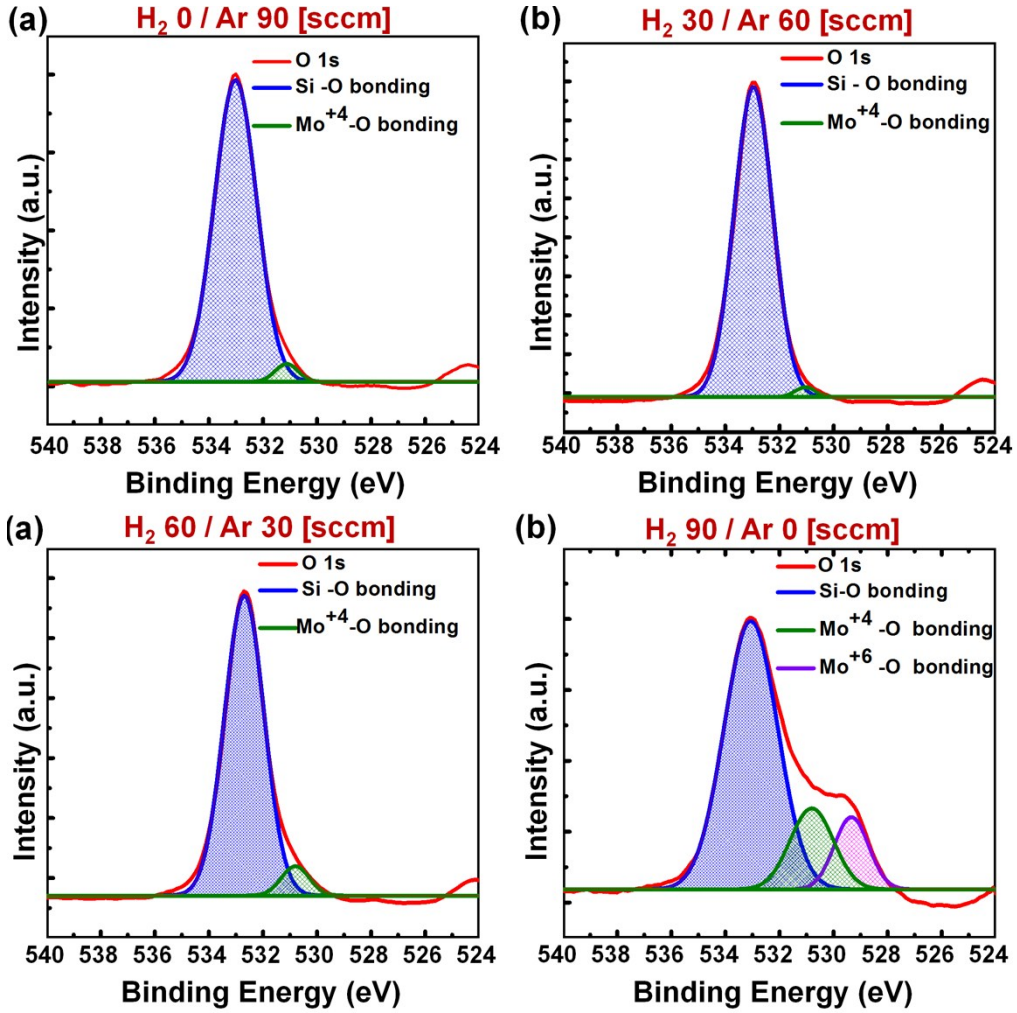

Figure S3. XPS O 1s spectra obtained under (a) 0 sccm, (b) 30 sccm, (c) 60 sccm, and (d) 90 sccm H_2 conditions.

Edge Configuration in the DFT Models: We studied the energy requirements for MoS_2 growth under different growth atmosphere conditions using density functional theory (DFT) calculation methods. Results from previous XPS and STM studies [4-6] were used to design various edge configurations under different hydrogen flow rate conditions. Case 1 shows that each edge Mo atoms were covered with S dimers. The Case 1 configuration was stable under an abundant S synthesis atmosphere. Case 2 revealed two Mo atoms at each edge connected to one S atom. This configuration was stable under S-deficient (or H_2-abundant) conditions. Case 3 revealed that each Mo edge atom was connected to one O atom due to partial oxidization under abundant H_2 conditions.

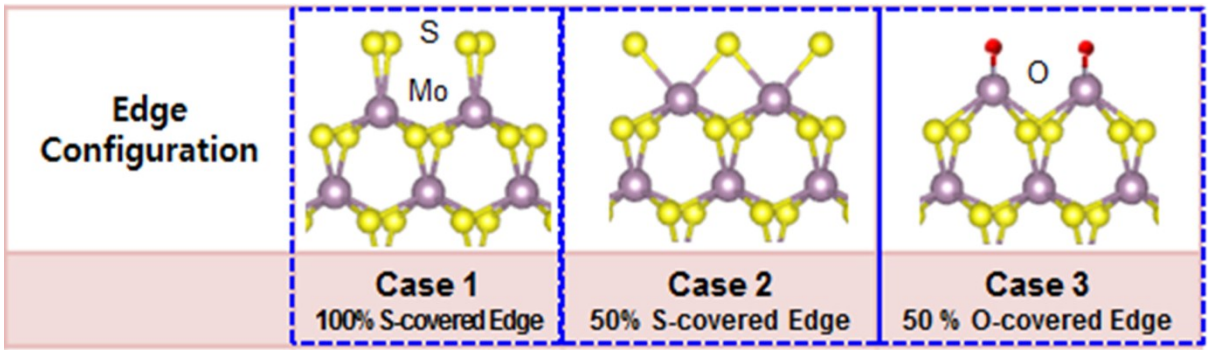

Figure S4. Edge configurations in the DFT models. Case 1: 100% S-covered edge; Case 2: 50% S-covered edge; Case 3: 50% O-covered edges. The purple, yellow, and red spheres indicate molybdenum, sulfur, and oxygen atoms, respectively.

Non-volatile memory prepared with a MoS_2 nanoparticle floating gate: The I_{DS}–V_{CG} transfer curves obtained from a device prepared without a floating gate revealed a negligible V_{th} shift between the program and erase states (Supplementary Figure S5). This device was fabricated using a few-layer MoS_2 channel that had been e-beam deposited onto a 10 nm SiO_2 layer supported by a 90 nm SiO_2/Si substrate as a tunnel oxide. No other floating gate layers were present between the control oxide and the tunnel oxide. Supplementary Figure S6 shows the I_{DS} – V_{CG} transfer curves measured from memory devices prepared with 5 different floating gates. Each floating gate displayed several shifted V_{th} values in the range 2–8 V for the program and erase states. The memory device prepared with a 5 nm MoS_2 nanoparticle floating gate exhibited a large memory window due to the high fraction of edge states. The average memory windows were estimated from several fabricated memory devices prepared with 5 different floating gates (Supplementary Figure S7). The memory windows of each device depended on the MoS_2 nanoparticle size in the floating gate. The average memory window increased as the MoS_2 nanoparticle size decreased due to an increase in the presence of trap states from the MoS_2 edge as the MoS_2 nanoparticle size decreased.

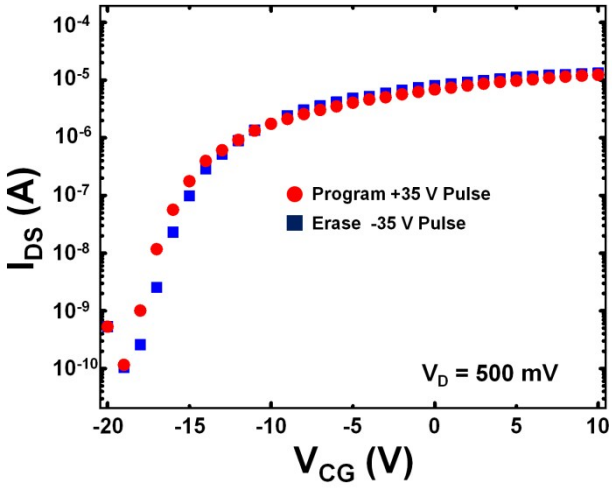

Figure S5. I_{DS} – V_{CG} transfer characteristics measured from the MoS_2 back-gate FET prepared without a floating gate.

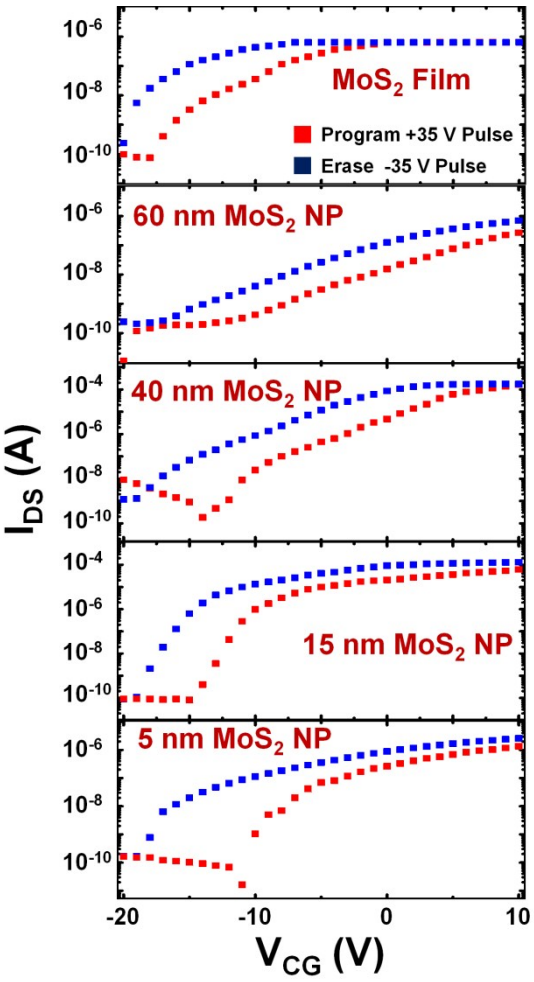

Figure S6. I_{DS} – V_{CG} transfer curves obtained from the memory devices prepared with various floating gates.

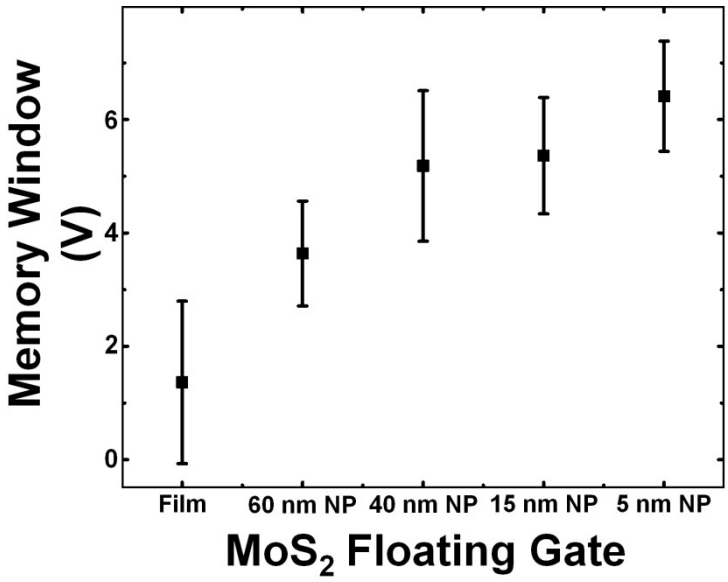

Figure S7. Average memory windows obtained from the different floating gates.

References

1. C. Lee, H. Yan, L. E. Brus, T. F. Heinz, J. Hone and S. Ryu, *ACS Nano*, 2010, **4**, 2695-2700.
2. M. Ivanda, S. Musić, M. Gotić, A. Turković, A. M. Tonejc and O. Gamulin, *Journal of Molecular Structure*, 1999, **480–481**, 641-644.
3. P. A. Spevack and N. S. McIntyre, *The Journal of Physical Chemistry*, 1993, **97**, 11031-11036.
4. T. F. Jaramillo, K. P. Jørgensen, J. Bonde, J. H. Nielsen, S. Horch and I. Chorkendorff, *Science*, 2007, **317**, 100-102.
5. J. V. Lauritsen, M. V. Bollinger, E. Lægsgaard, K. W. Jacobsen, J. K. Nørskov, B. S. Clausen, H. Topsøe and F. Besenbacher, *Journal of Catalysis*, 2004, **221**, 510-522.
6. J. V. Lauritsen, J. Kibsgaard, S. Helveg, H. Topsoe, B. S. Clausen, E. Laegsgaard and F. Besenbacher, *Nat Nano*, 2007, **2**, 53-58.